Available online at www.sciencedirect.com
ScienceDirect
Journal of the European Ceramic Society 26 (2006) 3665–3673
www.elsevier.com/locate/jeurceramsoc

Sintering behaviour of $La_{1-x}Sr_xFeO_{3-\delta}$ mixed conductors

Lise T. Sagdahl, Mari-Ann Einarsrud, Tor Grande *

Department of Materials Science and Engineering, Norwegian University of Science and Technology, 7491 Trondheim, Norway

Received 1 November 2005; received in revised form 18 January 2006; accepted 28 January 2006
Available online 10 March 2006

Abstract

The sintering properties of $La_{1-x}Sr_xFeO_{3-\delta}$ ($x = 0.1$, 0.25) mixed conductors have been investigated with particular emphasis on the effect of secondary phases due to cation non-stoichiometry (±5 mol% La excess and deficiency). Secondary phases, located at grain boundaries in cation non-stoichiometric materials, increased the sintering temperature compared to single-phase materials. Extensive swelling in final stage of sintering was observed in all materials, which resulted in micro-porous materials. The swelling was most pronounced in the phase pure and two-phase materials due to La-deficiency, while refractory secondary phases in La-excess materials inhibited both sintering, grain growth and swelling. In La-deficient materials, formation of molten secondary phases resulted in rapid swelling due to viscous flow. The present findings demonstrated the importance of controlling sintering temperature and time, as well as careful control of the cation stoichiometry of $La_{1-x}Sr_xFeO_{3-\delta}$ in order to achieve fully dense and homogenous $La_{1-x}Sr_xFeO_{3-\delta}$ ceramics.

Keywords: Perovskites; Sintering; Porosity; Membranes; Fuel cells; (La, Sr)FeO_3

1. Introduction

Perovskite materials such as $La_{1-x}Sr_xFeO_{3-\delta}$ (LSF) become oxygen deficient at elevated temperature and have a significant oxygen ion and electronic conductivity.[1] These mixed conducting oxides have potential applications as gas sensors, oxygen permeable membranes, electrodes and oxidation catalysts.[2–8] Dense materials with sufficient mechanical and chemical stability are required for these applications, and knowledge of the sintering properties of the materials is important. Sintering of $LaFeO_3$ powders has shown that small amounts of secondary phases in the materials affect the densification behaviour considerably.[9] The densification behaviour of $La_{1-x}Sr_xFeO_{3-\delta}$ has to our knowledge not been studied extensively, but reports on $SrFeO_{3-\delta}$ ceramics[10–13] show low densities and swelling at higher temperatures. Kleveland et al.[11] have emphasized the importance of good control of the cation stoichiometry to avoid post sintering swelling. The swelling was caused by reductive heterogeneous phase equilibria involving secondary phases resulting in oxygen evolution and pore expansion.

Here, we present a systematic study of the sintering properties of $La_{1-x}Sr_xFeO_{3-\delta}$ ceramics. Particular attention is given to the role of secondary phases due to offset from nominal cation stoichiometry and moreover post sintering swelling due to pore expansion.

2. Experimental

Stoichiometric powders with nominal composition $La_{0.9}Sr_{0.1}FeO_3$ and $La_{0.75}Sr_{0.25}FeO_3$ were prepared by spray drying (Bűchi, Mini spray-Drier B-191) of solutions of glycine and nitrates as described by Fossdal et al.[14] La-excess and La-deficient powders were also prepared by the same method, the nominal compositions are summarized in Table 1. The resulting powders were ball-milled (Si_3N_4-balls) for 20 h in iso-propanol, before calcining in air at 900 °C for 24 h. Some of the $La_{0.75}Sr_{0.25}FeO_3$ powder was subsequently calcined at 1050 °C in order to obtain a coarsened powder. The surface area of the calcined powders was measured by nitrogen adsorption (ASAP 2000, Micromeritics).

Powder pellets (0.5–0.8 g) were prepared by uniaxial pressing at 230–250 MPa. The relative green density measured using geometrical dimensions and weight was in the range 56–61% of theoretical density. Uniaxially pressed pellets were sin-

* Corresponding author. Tel.: +47 73 59 40 84
E-mail address: Tor.Grande@material.ntnu.no (T. Grande).

0955-2219/$ – see front matter © 2006 Elsevier Ltd. All rights reserved.
doi:10.1016/j.jeurceramsoc.2006.01.013

tered in air at 1050–1550 °C for 2–24 h. Heating and cooling rates were 200 K/h. The density of sintered pellets was measured by Archimedes technique using iso-propanol. The open and closed porosity was calculated using a theoretical density of 6.57 and 6.17 g/cm^3 for respectively $La_{0.9}Sr_{0.1}FeO_3$ and $La_{0.75}Sr_{0.25}FeO_3$.[15]

Dilatometry (Netzch DIL 402C) was performed on uniaxially pre-pressed and further cold isostatic pressed (200 MPa) pellets in a vertical direction. The pellets had green densities close to 60% of theoretical. Dilatometry was performed in flowing air at a heating rate of 120 K/h or at isothermal conditions for up to 30 h. The force acting on the powder compact correspond to a pressure of 300 Pa. Thermal gravimetrical analysis (Netzcsh STA 449C) was performed in synthetic air on powder samples in the temperature interval 20–1450 °C. Heating and cooling rates were 120 K/h.

Microstructural analysis of fractured cross sections of the sintered pellets was performed using a scanning electron microscope, SEM (Zeiss DSM 940) and energy dispersive spectroscopy (EDS) (Noran Instruments, Tracor Series II). Fractured and polished cross sections of the sintered pellets were also investigated by optical microscopy (Reichert-Jung, MeF3-metallograph) coupled to a digital camera (Sony DKC-5000). The polished surfaces were prepared by grinding with SiC-papers followed by polishing with diamond particles down to 1 μm.

X-ray powder diffraction (XRD) was performed on a Siemens D5005 diffractometer (Cu Kα radiation and a secondary monochromator) in the 2θ range 15–80° with step 0.02° and step time 25.0 s. Cell parameters and crystallographic densities were calculated from the X-ray diffraction diagrams.

3. Results

3.1. Characterization of the powders

The nominal composition, surface area and phase composition of the six different powders are summarized in Table 1. The two stoichiometric materials (La09 and La075) were phase pure according to XRD and the unit cell parameters were in good accord with literature.[14,15] The four non-stoichiometric materials (La09, La085, La80 and La65) contained secondary phases in accord with the nominal stoichiometry and phase diagrams of the system SrO–La_2O_3–Fe_2O_3 reported by Fossdal et al..[16] In La085 the secondary phase changed from Fe_2O_3 in the calcined powder to $La_{1-x}Sr_x$ $Fe_{12}O_{19}$ in the sintered specimens, which is also in accord with the phase diagrams.[16] Generally, the diffraction lines of the secondary phases were easier to observe in sintered samples compared to the powders due to particle size broadening and reactions with moisture, which was particularly a problem with the powders containing La_2O_3 as secondary phase. The average particle size of the powders calculated from the surface area assuming spherical morphology, given in Table 1, was confirmed by electron microscopy.

3.2. Densification and post sintering swelling studied by dilatometry

The linear shrinkage and differential linear shrinkage of stoichiometric La09 and non-stoichiometric La085 and La095 powders during heating are shown in Fig. 1. The region with negative differential shrinkage will be commented first. There are no systematic relationship between the sintering properties and the initial particle size (Table 1). The difference in sintering behaviour is caused by the presence of secondary phases in the La085 and La95 powders. Sintering of phase pure La09 was initiated at 780 °C, about 40 K lower than compared to La085 and La95. Moreover, better sintering properties of La09 is also reflected by the larger negative differential linear shrinkage. A single sintering event is evident from the linear differential shrinkage and a single dominant sintering mechanism is therefore inferred for La09. Two densification processes are evident for La085, see Fig. 1. Similar behaviour was also observed for similar materials containing secondary phases. The apparent 1% reduction in the linear shrinkage of La095 between 1270 and 1350 °C was reproduced in a second experiment.

A pronounced reduction of the density was observed at higher sintering temperatures for all three materials. The materials reached a maximum density at the temperature where the differential linear shrinkage changed sign, see Fig. 1. The temperature, corresponding to the maximum density, was shifted upward for La095 and La085 containing secondary phases. This reflects the poorer sintering properties of these two powders relative to the phase pure La09. In the region where the differential linear shrinkage is positive the materials were swelling resulting in a lower density. Moreover, the maximum expansion rate (posi-

Table 1
Chemical and physical properties of powders; nominal composition, Label, secondary phases, surface area and estimated particle size from surface area assuming spherical particles

Label	Nominal composition	Secondary phases	Estimated content of sec. phases (wt%)	Surface area (m^2/g)	Particle diameter[a] (μm)
La09	$La_{0.9}Sr_{0.1}FeO_{3-\delta}$	None	0	3,69	0.12
La085	$La_{0.85}Sr_{0.1}FeO_{3-\delta}$	$Fe_2O_3La_{1-x}Sr_xFe_{12}O_{19}$[b]	1.7	1.97	0.23
La095	$La_{0.95}Sr_{0.1}FeO_{3-\delta}$	La_2O_3	3.3	6.21	0.07
La075	$La_{0.75}Sr_{0.25}FeO_{3-\delta}$	None	0	3.14/1.26[a]	0.16/0.39[a]
La065	$La_{0.65}Sr_{0.25}FeO_{3-\delta}$	$La_{1-x}Sr_xFe_{12}O_{19}$	3.7	2.30	0.21
La080	$La_{0.80}Sr_{0.25}FeO_{3-\delta}$	$La_2SrFe_2O_{7-\delta}$	11.1	5.64	0.09

[a] Powder calcined at 1050 CircC after calcination at 900 CircC.
[b] Observed in sintered specimens.

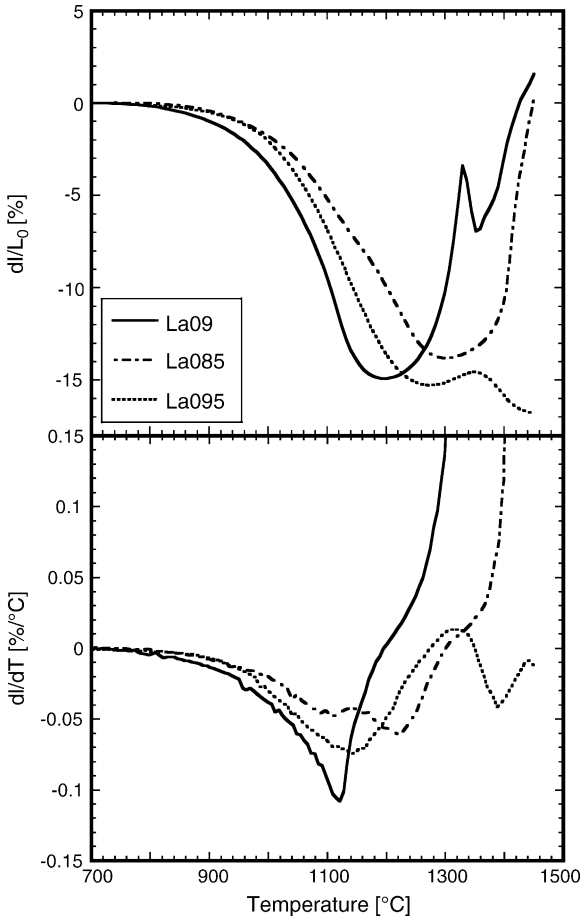

Fig. 1. Temperature dependence of linear shrinkage and differential linear shrinkage for the La09-series: La09, La085 and La095. The heating/cooling rates were 120 K/h. The samples were held for 1 h at 1450 °C before cooling. The densities of the samples after heating to 1450 °C and cooling to room temperature were 3.43, 3.07 and 5.85 g/cm^3, respectively. The small increase in density at about 1350 °C for La09 is due to deformation of the sample by the pressure (300 Pa) from the push-rod in the dilatometer.

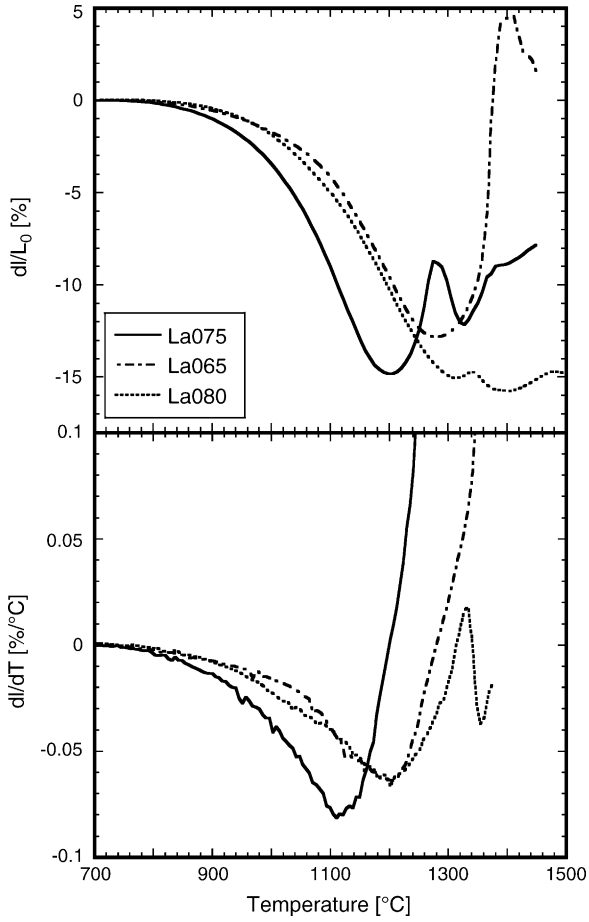

Fig. 2. Temperature dependence of linear shrinkage and differential linear shrinkage for the La075-series: La075, La065 and La080 (25% Sr). The heating/cooling rates were 120 K/h. The samples were held for 1 h at 1450 °C before cooling. The densities of the samples after heating to 1450 °C (1500 °C for La080) and cooling to room temperature were 3.70, 2.84 and 5.94 g/cm^3, respectively.

tive d*l*/d*T*) during de-sintering is far higher than the maximum shrinkage rate observed during sintering. In some cases the final density was reduced below the initial green density. The abrupt change in the linear shrinkage, as observed for La09 during the swelling period, was also observed for other samples, see Fig. 2. This is caused by pore wall rupture as discussed further below.

The linear shrinkage and differential linear shrinkage of phase pure La075 powder and La065 and La080 powders, containing secondary phases, are shown in Fig. 2. The sintering behaviour and post sintering swelling is strikingly similar to the observations shown in Fig. 1. Again the sintering and post sintering swelling was suppressed to higher temperatures due to the presence of secondary phases.

The onset for sintering of the single-phase powder La075 with the highest sintering rate is 740 °C. This was 40 degrees lower than for single phase La09, which reflects that the sintering temperature is decreasing with increasing Sr content in $La_{1-x}Sr_xFeO_{3-\delta}$. This decrease is also in line with the sintering behaviour reported for $LaFeO_3$[9] and $SrFeO_{3-\delta}$.[11] As for La09 (Fig. 1), a single sintering event was observed for La075, as shown in Fig. 2.

The cylinder-shaped specimens were significantly deformed after the dilatometer experiments. The diameter at the middle of the cylinders was significantly larger than at the edges. The expansion was clearly suppressed in the direction towards the push rods of the dilatometer.

3.3. Microstructure and porosity

The densification of the six materials was further investigated at isothermal conditions in the temperature interval 1050–1550 °C. The density of the materials after 2 h sintering is shown in Figs. 3 and 4 as a function of the sintering temperature. The density of the two single-phase materials La09 (Fig. 3) and La075 (Fig. 4) reached a maximum relative density of about 90–91% of the theoretical between 1100 and 1150 °C before the density decreased quite dramatically at higher sintering temperatures. These observations confirmed the trends observed by dilatometry (Figs. 1 and 2). The pronounced effect of the

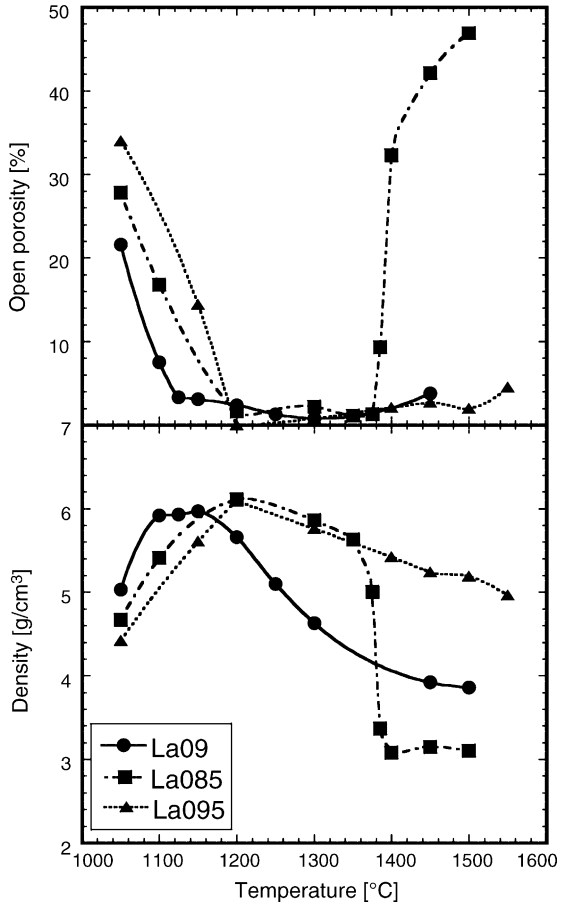

Fig. 3. Temperature dependence of the open porosity and the absolute density after 2 h isothermal sintering for the La09 series: La09, La085 and La095. The lines are guides to the eye.

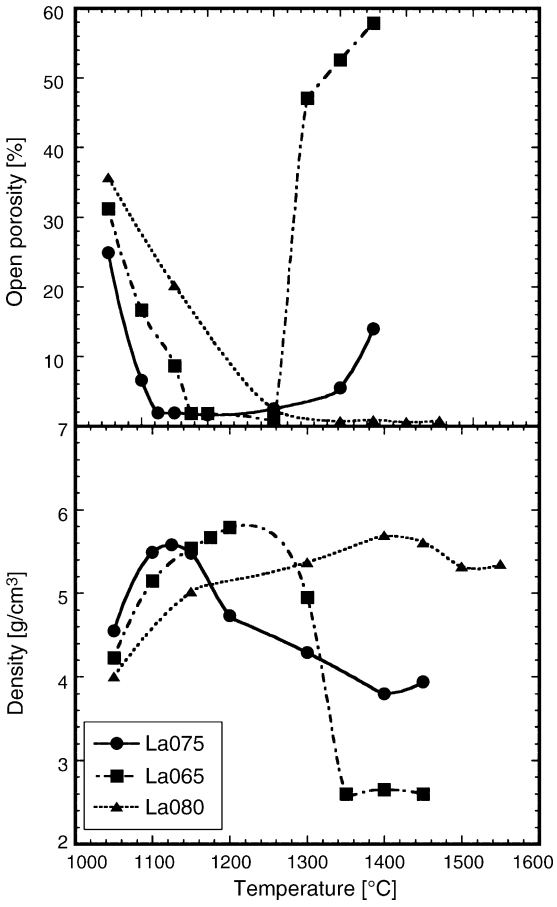

Fig. 4. Temperature dependence of the open porosity and the absolute density after 2 h isothermal sintering for the La075-series: La075, La065 and La080. The lines are guides to the eye.

minority phases on the densification was again evident. The maximum density of the materials containing secondary phases was obtained at significantly higher sintering temperatures relative to the phase pure materials. Moreover, the La-deficient materials (La085 and La065) became significantly less dense at high sintering temperatures, and in some cases the final density became even lower than the initial green density. A dramatic reduction in the density was observed for the La-deficient materials La085 (Fig. 3) and La065 (Fig. 4) at about 1380 and 1320 °C, respectively.

The open porosity of the specimens, obtained by Archimedes method, is also shown together with the density in Figs. 3 and 4. The open porosity is strongly declining with increasing density and become close to zero at the maximum density. The residual porosity of about 9–10% at the maximum density is essentially closed for all six materials. The decreasing density at higher sintering temperatures is initially only caused by an increasing closed porosity as shown in Figs. 3 and 4.

The microstructure of La075 ceramics sintered at 1200 °C is shown in Fig. 5. The microstructure is homogeneous on a μm scale and considerable porosity is evident as expected from the low relative density (90%). The porosity is evenly distributed and the average pore size is less than 1 μm. Pores have generally spherical morphology with concave curvature and are only sur-

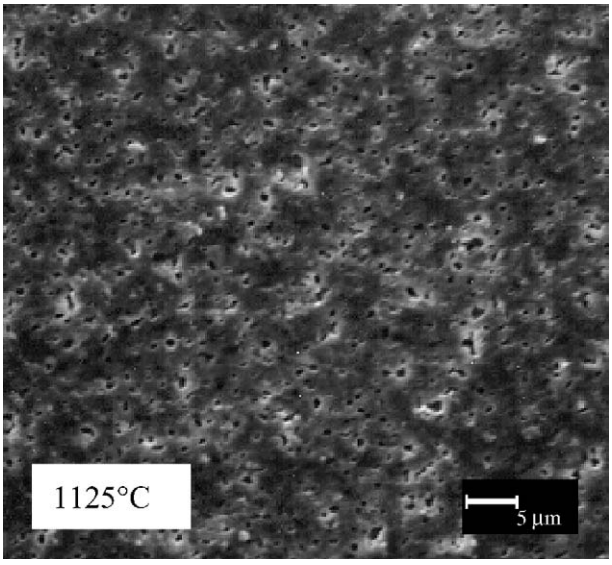

Fig. 5. SEM image of polished surface of La075 after sintering in air at 1125 °C for 2 h.

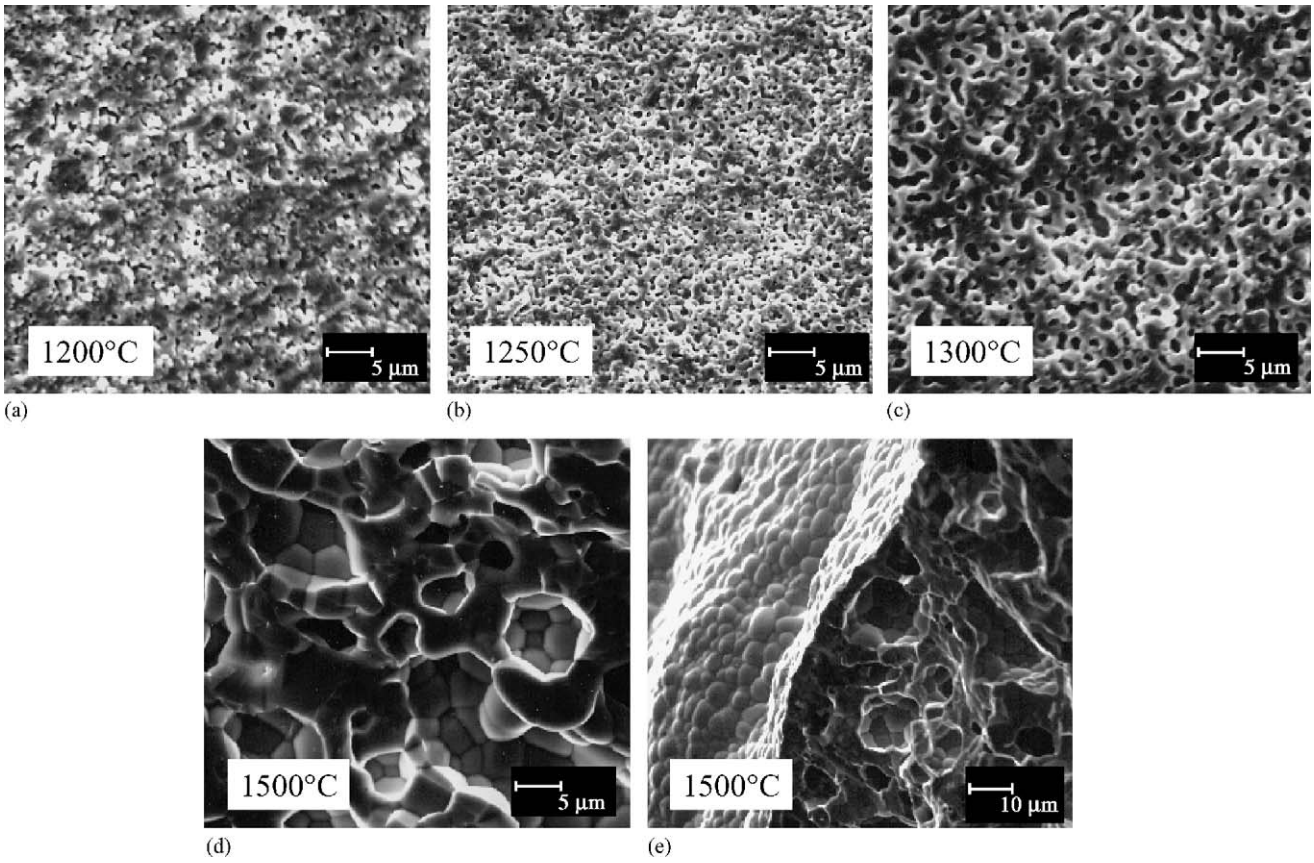

Fig. 6. SEM images of fracture surfaces of La09 after sintering in air at (a) 1200 °C, (b) 1250 °C, (c) 1300 °C, (d) 1500 °C, for 2 h, respectively. (e) SEM image of fracture surface and sample surface of La09 after sintering in air at 1500 °C for 2 h.

rounded by 3–4 grains. The apparent grain size is sub-micron and no significant grain growth had occurred at this temperature. The microstructure of the other materials at the maximum density was essentially identical, except for the presence of the minority phase on grain boundaries in materials with cation non-stoichiometry.

The microstructure of La09 sintered at four different temperatures between 1200 and 1500 °C is shown in Fig. 6. These SEM images illustrate the microstructure development during the swelling process. The grain size increases from less than 1 μm at 1200 °C to 5–10 μm at 1500 °C. The grains appear equiaxed in all images. More striking is the expansion of the pores from spherical pores less than 1 μm in diameter encircled by a few grains at 1200 °C, to intricate pore networks with a convex curvature of the pore surfaces at 1500 °C. The pore expansion and grain growth were uniform throughout the specimen. There could not be observed any variation in the microstructure even in the vicinity of the outer surface of the samples, see Fig. 6e. The porosity was essentially closed as evidenced by the closed surface shown in Fig. 6e. Inspection of several fractured surfaces of the porous materials revealed that only a single layer of grains separated large pores from the outer surface. Note also that the curvature of the pore surface and the outer surface was similar for the porous samples fired at high temperatures.

The microstructure of La075 was essentially similar to La09. The swelling process was governed by expansion of the evenly distributed pores. The swelling process was accompanied by grain growth, and pore ripening or coalescence was also evident, as nearly all pores have become larger than the average grain size.

The rapid development of open porosity in the final stage of swelling was due to pore expansion as illustrated in the SEM images of La085 in Fig. 7. The abrupt swelling is reflected in the extreme pore expansion from 1375 to 1400 °C. Plate-like grains identified as the secondary phase $La_{1-x}Sr_xFe_{12}O_{19}$, can be observed by SEM in backscatter mode at sintering temperatures from about 1200 °C (Table 1). Like the perovskite grains, grains of $La_{1-x}Sr_xFe_{12}O_{19}$ became larger with increasing temperature. At 1500 °C, the plate-like grains of $La_{1-x}Sr_xFe_{12}O_{19}$, indicated by the arrow in Fig. 7, were about 10 μm in length. The length of these plate-like grains seamed to by limited by the pore size.

The microstructure of La065 materials observed with increasing temperature mimics the development observed for La085. The decreasing density and increasing open porosity above 1300 °C were accompanied by an abrupt increase in the average pore diameter. A systematic SEM/EDS investigation showed that $La_{1-x}Sr_xFe_{12}O_{19}$ was present as scattered particles from 1150 °C. Above 1300 °C the temperature region of

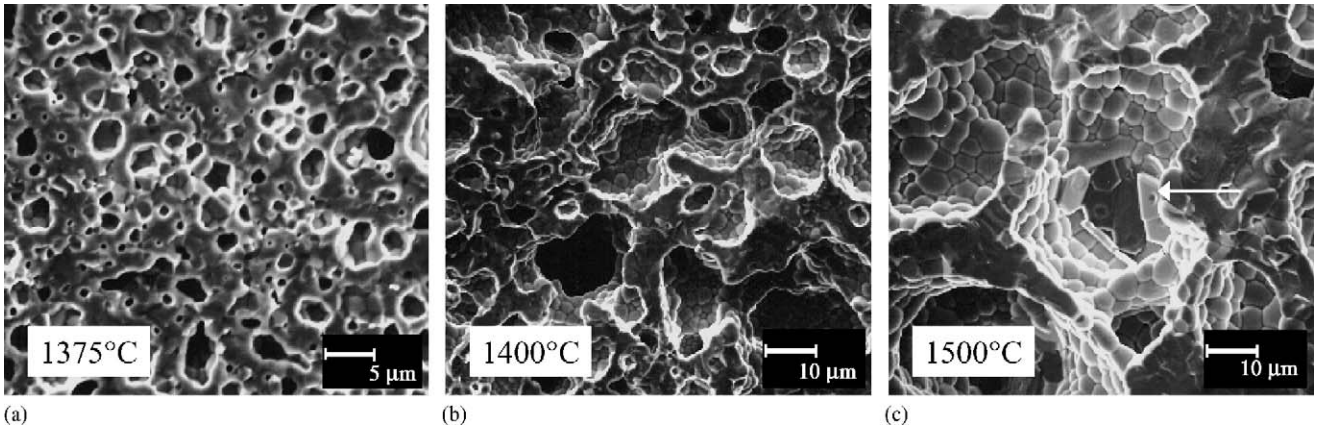

Fig. 7. SEM images of fracture surfaces of La085 after sintering in air at (a) 1375 °C, (b) 1400 °C and (c) 1500 °C for 2 h, respectively. The arrow in (c) points to the secondary phase (La,Sr)$Fe_{12}O_{19}$.

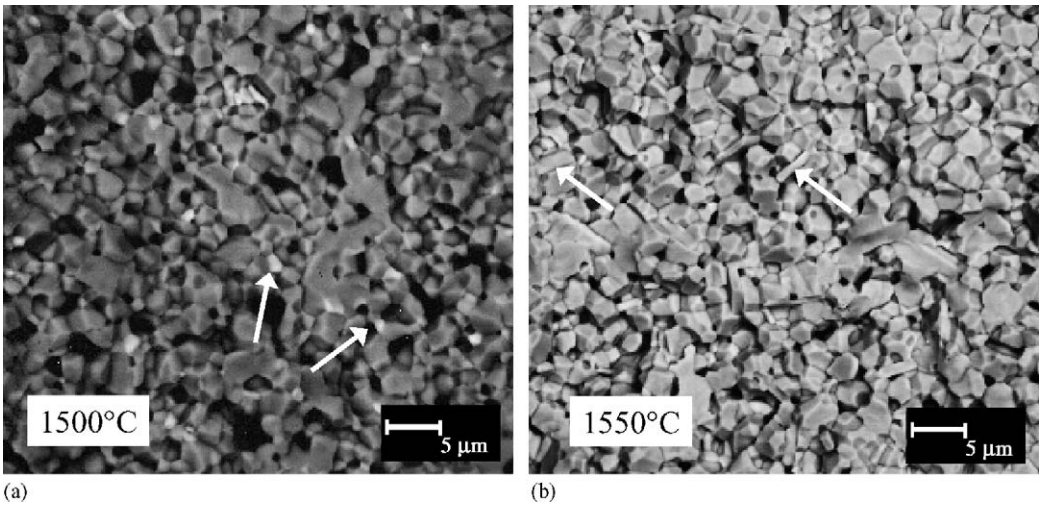

Fig. 8. (a) SEM image (back scatter) of fracture surface of La095 after sintering in air at 1500 °C for 2 h. The light grains indicated by the arrows are La_2O_3. (b) SEM image (back scatter) of fracture surface of La080 after sintering in air at 1550 °C for 2 h. The needle like grains, indicated by the arrows, is $Sr_2LaFe_2O_{7-\delta}$.

the most pronounced swelling, a significant grain growth of $La_{1-x}Sr_xFe_{12}O_{19}$ had occurred.

In the case of La-excess materials, La095 and La080, the swelling was considerably less pronounced. This is easily recognized both by dilatometry (Figs. 1 and 2) and the isothermal sintering experiments (Figs. 3 and 4). The microstructure for the La-excess sample, La095, at 1500 °C shown in Fig. 8a, is fundamentally different from the porous samples described so far. The minority phase La_2O_3 can be identified as brighter grains with a diameter of about 1 μm distributed between the perovskite grains. The grain size of the perovskite phase is less than 3–4 μm in diameter and the pore diameter is less than about 2 μm. Both grain growth and pore growth was hindered by the presence of La_2O_3. La080 sintered at 1550 °C (Fig. 8b) had a microstructure similar to La095, but here the secondary phase, identified as $La_2SrFe_2O_{7-\delta}$ by XRD, had a plate-like structure (indicated by arrows). Better contrast between the perovskite phase and $Sr_{3-x}LaFe_2O_7$ was obtained by optical microscopy. This secondary phase was observed in samples sintered from 1300 to 1550 °C by XRD, SEM/EDS and optical microscopy.

4. Discussion

4.1. Phase composition and oxygen non-stoichiometry

The secondary phases observed in the cation non-stoichiometric samples were in accord with the SrO-La_2O_3-Fe_2O_3 phase diagram.[16] The extensive swelling of La085 and La065 were caused by the formation of a liquid phase due to presence of the secondary phases Fe_2O_3 and $La_{1-x}Sr_xFe_{12}O_{19}$. The formation of the liquid phase at Fe-excess relative to $La_{1-x}Sr_xFeO_{3-\delta}$ as for La085 and La065 is also previously reported.[16] The rapid swelling observed at 1380 and 1320 °C for La085 and La065 can be interpreted as the solidus temperature in the pseudo binary systems $La_{1-x}Sr_xFe_{12}O_{19}$–$La_{1-y}Sr_yFeO_{3-\delta}$. An increasing solidus temperature with increasing Sr-content is in line with the Gibbs phase rule and is also in line with previous observations of solidus temperatures.[16]

Mizusaki et al.[1] have shown that LSF materials become oxygen deficient at elevated temperatures due to the heterogeneous

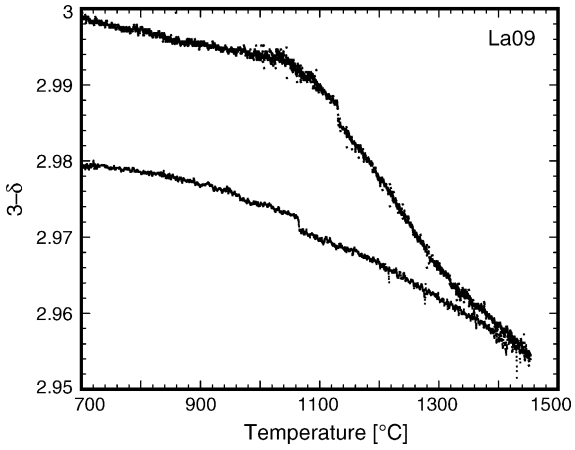

Fig. 9. Oxygen non-stoichiometry vs. temperature for La09. The material was assumed to be stoichiometric at ambient temperature.

phase equilibrium:

$$La_{1-x}Sr_xFeO_3 = La_{1-x}Sr_xFeO_{3-\delta} + \frac{\delta}{2}O_2\,(g).$$

The oxygen non-stoichiometry in air above 1200 °C is not known, and we therefore conducted a thermogravimetrical analysis of La09 up to 1450 °C. The oxygen non-stoichiometry versus temperature at constant heating and cooling rates measured by thermal gravimetrical analysis for the single-phase sample, La09, is given in Fig. 9. The material is assumed stoichiometric ($\delta = 0$) at room temperature in accord with literature.[1] The weight loss upon heating corresponds to a change in δ of about 0.03 in the temperature interval 1100–1450 °C. The data demonstrates that the sintered sample departs from equilibrium oxygen content during cooling. We expect a similar behaviour for the five other materials studied here.

After calcination of the La-excess La095 powder, La_2O_3 was detected by XRD in addition to the perovskite (Table 1). La_2O_3 was observed to be hygroscopic and hydroxides were formed in powders made from the sintered materials, as well as in calcined powders. It is worth noting that La_2O_3 might cause the sintered materials to disintegrate when stored in air as observed for $LaFeO_3$ ceramics [9].

Initially, we were concerned that the unusual swelling phenomena were in part due to decomposition of small amounts of impurities like $SrCO_3$ or $SrSO_4$ that would lead to evolution of gases upon heating and hence cause pore expansion. However, IR-spectroscopy on selected powders below and above the temperature of the swelling gave no evidence for IR-absorption due to carbonates, sulphates or any components that would result in volatile gaseous impurities.

4.2. Densification

From Figs. 1–4 it is evident that the presence of minority phases strongly influenced the sintering rate, and that the small variation in the average grain size of the materials (Table 1) can not explain the difference in sintering behaviour. According to solid state sintering theory[17] the densification rate by grain boundary diffusion and volume diffusion is proportional to d^{-4} and d^{-3}, respectively, where d is the average particle diameter. Figs. 1 and 2 show that the single-phase powders (La09 and La075) had the highest sintering rate even though the average grain size was larger than for La-excess powders (La085 and La065). Densification is also initiated at a lower temperature for the single-phase powders (Figs. 1 and 2). We can therefore conclude that within the small variation in the particle size (Table 1), the sintering properties of the six powders were determined by the phase composition. The four powders containing two phases sintered at a higher temperature relative to the two powders containing only a single phase. These observations are consistent with our work on $LaFeO_3$,[9] where La_2O_3 was observed to inhibit sintering, especially at low temperatures.

Only a single sintering event was observed by dilatometry on the single-phase materials La09 and La075 (Figs. 1 and 2). This is also consistent with dilatometric studies of pure $LaFeO_3$ and $SrFeO_{3-\delta}$ powders.[9–11] The initial sintering temperature is increasing going from pure $LaFeO_3$ and $SrFeO_{3-\delta}$, reflecting the difference in the melting temperature of the two pure compounds. So far it has not been possible to determine if the solid state sintering is governed by cation diffusion along grain boundaries or by bulk diffusion. Grain boundary diffusion is usually dominating at low temperature in ceramics[17] and cation diffusion in $LaFeO_3$ has given evidence for much faster cation grain boundary diffusion than bulk diffusion.[18] Our findings have shown that sintering in these materials is very sensitive to grain boundary chemistry (secondary phases at the grain boundaries), which may also effect the grain boundary diffusion.

The presence of Fe_2O_3 in the La085 powders demonstrated that Fe_2O_3 also behaves as a sintering inhibitor as the sintering rate was significantly lower than for the single phase powder La09 (Fig. 1). Two sintering events were also evident for La085 in contrast to the single event observed for La09. A possible explanation for the two events were the gradual transformation of Fe_2O_3 to $La_{1-x}Sr_xFe_{12}O_{19}$ in line with expectations from phase diagrams.[16] The suppression of the densification rate between 1100 and 1200 °C for La085 can, hence, be explained by the formation of $La_{1-x}Sr_xFe_{12}O_{19}$ from Fe_2O_3 and the perovskite, which was observed by SEM from about 1150 °C. This explanation is supported by the sintering behaviour of the La065 powder, in which $La_{1-x}Sr_xFe_{12}O_{19}$ is the equilibrium secondary phase after calcination. For La065 only a single sintering event was observed (Fig. 2). Finally, the low sintering rate for La065 shows that also $La_{1-x}Sr_xFe_{12}O_{19}$ acts as a sintering inhibitor. In the La-excess materials the secondary phases inhibited both sintering, grain growth and swelling.

4.3. Post sintering swelling and microstructure

The sintering properties of the six powders presented here have revealed the difficulties of obtaining dense ceramics of mixed valence state oxides due to swelling in the final stage of sintering. Extreme expansion during sintering has also been reported for other related perovskites by the present group[9,11] and others groups.[10,12] It is worth noting that swelling is also observed in ceramics of high-T_c superconductors[19–20] where the valence state of Cu is reduced during sintering. However, even

though we can conclude that evolution of O_2 is indeed occurring during sintering of both these type of materials, this does not need to cause swelling. The swelling of our materials was initiated above 1200 °C, which coincide with the corresponding swelling observed for $SrFeO_3$-based materials.[11]

In conventional sintering theory porosity may increase at high temperatures due to grain growth accompanied by pore coalescence or by pore ripening.[17] The final porosity is determined by the total amount of gas trapped in the pores at pore closure and a may cause an increase in porosity of about 5–8%.[21] If the gas trapped in the closed pores is soluble in the bulk ceramic the effect should be less pronounced. Pore coalescence and pore ripening alone can therefore not explain the present observations.

The microstructure of La09 (Fig. 6) shows that the pores at 1200 °C have concave pore surfaces, and they are therefore unstable and should contract and finally disappear if they were filled with pure oxygen since the materials are oxygen permeable (require slow grain growth). The swelling upon further heating results in an intricate pore structure with convex pore surfaces. However, the transition from pores with concave to convex curvature and the drastic increase in the pore volume calls for an extraordinary explanation.

There are several observations in the literature which are relevant to the swelling phenomenon. Swelling or bloating of glasses due to decomposition of hydroxides or carbonates is a well-known phenomenon. We have excluded this possibility by IR-spectroscopy. Solid state foaming of titanium has been reported using hot-isostatic pressing of titanium powders in the presence of an inert gas such as argon, followed by expansion of the pores filled with high pressure argon at ambient pressure and elevated temperature.[22] The resulting microstructure of the porous titanium is strikingly similar to swollen materials reported here. Extensive swelling of Fe_2O_3[23] and expansion of bubbles in tableware and sanitary ware caused by evolution of O_2 due to reduction of Fe(III) to Fe(II), have also been reported.[24]

The involvement of gas evolution in the cases mentioned above has given us reasons to propose that the intrinsic evolution of O_2 during heating of $La_{1-x}Sr_xFeO_{3-\delta}$ is relevant for the observed pore expansion. However, the materials is known as reasonable oxygen permeation membranes[3,4] and one should expect that the oxygen evolved due to thermal reduction of iron should permeate out of the materials. The thermogravimetrical analysis (Fig. 9) shows that the cooling curve does not follow the heating curve. The oxygen permeation is therefore not as fast as we might expect. It is important to note that permeation measurements in air/helium gradients[3,5] mostly are conducted on polished samples, often after treating the surfaces in CO-containing atmosphere. The oxygen flux tends to increase significantly for long periods of time in absence of such pretreatment, which indicates a surface effect which needs to be investigated further. Temporary build up of oxygen pressure inside closed pores during heating might therefore give rise to a driving force for pore expansion. Considerable creep rates for related materials have been reported,[25,26] and only small overpressures of oxygen would therefore cause pore expansion.[27] The microstructure analysis reveals that grains remain equiaxed and no elongation of grains in the course of swelling is observed. The creep mechanism during swelling is therefore most likely diffusion accommodated grain boundary sliding in line find recent investigations on creep in related materials.[25,26] Some grain growth is observed during creep, which means that there is most likely a contribution of static/dynamic grain growth to the resultant creep behaviour.

The rapid pore expansion of the La-deficient materials La085 and La065 at 1380 and 1320 °C cannot be explained by the creep mechanism discussed above. Kleveland et al.[11] have reported fast swelling in Fe-excess $SrFeO_{3-\delta}$ based ceramics. The swelling coincided with the peritectic point in the $SrO–Fe_2O_3$ phase diagram.[28] The melting was reductive in nature and the simultaneous formation of a liquid phase and evolution of O_2 (g) caused a rapid expansion of the pores and grain growth due to viscous flow. As described previously, the presence of Fe_2O_3 rich secondary phases in La085 and La065 caused the formation of a liquid phase, which are related to the one observed by Kleveland et al.[11] We can therefore conclude that the rapid swelling of La085 and La065 observed at 1380 and 1320 °C is due to the formation of a secondary liquid phase.

The swelling phenomena of the La-excess materials La095 and La080 were significantly less pronounced than that of the other four materials (Figs. 1–4). This is in excellent agreement with the slow swelling observed in Sr-excess $SrFeO_{3-\delta}$ observed by Kleveland et al.[11] Only solid secondary phases were present in both cases. We can therefore conclude that refractory phases inhibit swelling as well as sintering and grain growth. Improved sintering behaviour have also been reported for $Sr(Fe,Al)O_3$-based ceramics by addition of Al_2O_3.[13]

4.4. Improving densification

Our observations show that the sintering competes with the swelling in these materials, which is confirmed by the low maximum density obtained by isothermal sintering for 2 h (Figs. 3 and 4). The high creep rate, combined with a closed pore structure and oxygen evolution, leads to low final density even in samples sintered for 48 h at temperatures where the sintering rate has its maximum. Sintering for long times will give higher final density only if the sintering rate is chosen so that most of the oxygen evolves before the pores close. By increasing the calcination temperature for La075 from 900 to 1050 °C, and sintering at 1200 °C for 30 h, a final density of 96.1% (5.93 g/cm^3) was obtained. The sintering temperature was 50 K below the maximum in the sintering rate, yet the sintering rate is high enough to obtain high-density materials. Similar results have been reported for $La_{0.5}Sr_{0.5}FeO_{3-\delta}$.[29]

5. Conclusions

The densification properties of stoichiometric and non-stoichiometric $La_{1-x}Sr_xFeO_{3-\delta}$ materials have been investigated. Secondary phases located at grain boundaries due to cation non-stoichiometry increased the sintering temperature and reduced the densification rate compared to single-phase

materials. Rather low density of the materials was achieved due to extensive swelling in final stage of sintering irrespective of the cation stoichiometry. The swelling was particularly rapid in the presence of liquid secondary phase. The driving force for the observed pore expansion is proposed to be due to a temporary over-pressure of oxygen in closed porosity caused by the thermal reduction of iron during heating. We have shown the importance of understanding the chemistry and heterogeneous phase equilibria in order to obtain dense ceramics of mixed conductors.

Acknowledgements

Financial support from The Norwegian Research Council and NTNU is acknowledged. We also thank Eli Beate Jakobsen for preparing some of the powders, Anita Fossdal and Gunn Torill Wikdahl for technical assistance and Elin Nilsen for performing the nitrogen adsorption measurements.

References

1. Mizusaki, J., Sasamoto, T., Cannon, W. R. and Bowen, H. K., Electronic conductivity and defect structure of $La_{1-x}Sr_xFeO_3$ (x = 0.1, 0.25). *J. Am. Ceram. Soc.*, 1983, **66**, 247–252.
2. Huang, K., Lee, H. Y. and Goodenough, J. B., Sr- and Ni-doped $LaCoO_3$ and $LaFeO_3$ perovskites: new cathode materials for solid oxide fuel cells. *J. Electrochem. Soc.*, 1998, **145**, 3220–3227.
3. van Hassel, B. A., ten Elshof, J. E. and Bouwmeester, H. J. M., Oxygen permeation flux through $La_{1-y}Sr_yFeO_3$ limited by carbon monoxide oxidation rate. *Appl. Catal. A: Gen.*, 1994, **119**, 279–291.
4. ten Elshof, J. E., Bouwmeester, H. J. M. and Verweij, H., Oxygen transport through $La_{1-x}Sr_xFeO_{3-\delta}$ membranes. I. Permeation in air/he gradients. *Solid State Ionics*, 1995, **81**, 97–109.
5. ten Elshof, J. E., Bouwmeester, H. J. M. and Verweij, H., Oxygen transport through $La_{1-x}Sr_xFeO_{3-\delta}$ membranes. II. Permeation in air/Co, CO_2 gradients. *Solid State Ionics*, 1996, **89**, 81–92.
6. Arakawa, T., Kurachi, H. and Shiokawa, J., Physicochemical properties of rare earth perovskite oxides used as gas sensor materials. *J. Mater. Sci.*, 1985, **20**, 1207–1210.
7. Carotta, M. C., Butturi, M. A., Martinelli, G., Sadaoka, Y., Nunziante, P. and Traversa, E., Microstructural Evolution of Nanosized Powders From the Thermal Decomposition of a Cyano-Complex for Thick Film gas sensors. *Sens. Actuators B*, 1997, **44**, 590–594.
8. Traversa, E., Matsushima, S., Okada, G., Sadoka, Y., Sakai, Y. and Watanabe, K., NO_2 sensitive $LaFeO_3$ thin films prepared by r.f. sputtering. *Sens. Actuators B*, 1995, **24–25**, 661–664.
9. Sagdahl, L. T., Einarsrud, M.-A. and Grande, T., Sintering of $LaFeO_3$ ceramics. *J. Am. Ceram. Soc.*, 2000, **83**, 2318.
10. Kokhanovskii, L. V., Vashuk, V. V., Vil'kotskaya, E. F., Vitushko, S. I. and Zinkevich, M. V., Synthesis, structure and some physiochemical properties of $SrCo_{1-x}Fe_xO_{3-\delta}$. *Inorg. Mater.*, 1999, **35**, 282–286.
11. Kleveland, K., Einarsrud, M.-A. and Grande, Sintering Behavior, Microstructure and Phase Composition of $(Sr(Fe\ Co)O_{3-\delta}$ Ceramics, T. *J. Am. Ceram. Soc.*, 2000, **83**, 3158–3164.
12. Kharton, V. V., Naumovich, E. N. and Nikolaev, V. A., Materials for high-temperature oxygen membranes. *J. Membr. Sci.*, 1996, **111**, 149–157.
13. Kharton, V. V., Shaula, A. L., Snijkers, F. M. M., Cooymans, J. F. C., Luyten, J. J., Yaremchenko, A. A. *et al.*, Processing, stability and oxygen permeability of $Sr(Fe, Al)O_3$-based ceramic membranes. *J. Membr. Sci.*, 2005, **252**, 215–225.
14. Fossdal, A., Menon, M., Wærnhus, I., Wiik, K., Einarsrud, M.-E. and Grande, T., Structural properties and thermal expansion of $La_{1-x}Sr_xFeO_{3-\delta}$ materials. *J. Am. Ceram. Soc.*, 2004, **87**, 1952–1958.
15. Dann, S. E., Currie, D. B., Weller, M. T., Thomas, M. F. and Al-Rawwas, A. D., The effect of oxygen stoichiometry on phase relations and structure in the system $La_{1-x}Sr_xFeO_3$ ($0 \le x \le 1.0$, $0 \le \delta \le 0.5$). *J. Solid State Chem.*, 1994, **109**, 134–144.
16. Fossdal, A., Einarsrud, M.-E. and Grande, T., Phase relations in the pseudo ternary system La_2O_3–SrO–Fe_2O_3. *J. Am. Ceram. Soc.*, 2005, **88**, 1988–1991.
17. German, R. M., *Sintering Theory and Practice*. John Wiley & Sons Inc., New York, 1996.
18. Wærnhus, I., Sakai, N., Yokokawa, H., Grande, T., Einarsrud, M.-E. and Wiik, K., Mass transport in $La_{1-x}Sr_xFeO_{3-\delta}$ (x = 0 and 0.1) measured by SIMS. *Solid State Ionics*, 2004, **175**, 69–71.
19. Kao, C. H., Dung, S. L., Lee, L. C., Wu, M. K., Chiu, Y. D. and Lei, T. S., Effects of starting powder with various high-T_c phase contents on the expansion of Bi–Pb–Sr–Ca–Cu–O pellets. *Mater. Sci. Eng. B*, 1994, **25**, 68–72.
20. Thayer, R. L., Schmidt, S. R., Dorris, S. E., Bullard, J. W. and Lanagan, M. T., Reactive sintering and retrograde densification of bulk bismuth-based superconductors. *J. Am. Ceram. Soc.*, 2000, **83**, 2365–2368.
21. German, R. M., Sintering atmosphere effects on the ductility of W–Ni–Fe heavy metals. *Metal. Trans. A*, 1984, **15**, 747–754.
22. Davis, N. G., Teisen, J., Schuh, C. and Dunand, D. C., Solid-state foaming of titanium by superplastic expansion of argon-filled pores. *J. Mater. Res.*, 2001, **16**, 1508–1519.
23. Nasr, M. I., Omar, A. A., Hessien, M. M. and El-Geassy, A. A., Carbon monoxide reduction and accompanying swelling of iron oxide compacts. *ISIJ Int.*, 1996, **36**, 164–171.
24. Kobayashi, Y., Ohira, O., Ohashi, Y. and Kato, E., Bending strength and microstructure of commercial porcelains for tablewares. *J. Ceram. Soc. Jpn.*, 1991, **99**, 495–502.
25. Kleveland, K., Wereszczak, A., Kirkland, T. P., Einarsrud, M.-A. and Grande, T., Compressive creep performance of $SrFeO_3$. *J. Am. Ceram. Soc.*, 2001, **84**, 1822–1826.
26. Majkic, G., Wheeler, L. T. and Salama, K., High-temperature deformation of $La_{02}Sr_{0.8}Fe_{0.8}Cr_{0.2}O_{3-\delta}$ mixed ionic–electronic conductor. *Solid State Ionics*, 2002, **146**, 393–404.
27. Finnie, L. and Heller, W. R., *Creep of Engineering Materials*. McGraw Hill Book Co. Inc., New York, 1959.
28. Fossdal, A., Einarsrud, M.-E. and Grande, T., Phase relations in the pseudo binary system SrO–Fe_2O_3. *J. Solid. State Chem.*, 2004, **177**, 2933–2942.
29. Diethelm, S., Van Herle, J., Sfeir, J. and Buffat, P., Correlation between oxygen transport properties and microstructure in $La_{05}Sr_{05}FeO_{3-\delta}$. *J. Eur. Ceram. Soc.*, 2005, **25**, 2191–2196.